Chapter 6

Assessment of foliar dust for environmental monitoring in an open cast iron ore mining areas

This Chapter has originally been published as: **Kayet, N**., Pathak, K., Chakrabarty, A., Kumar, S., Chowdary, V. M., Singh, C. P., & Basumatary, S. (**2019**). Assessment of foliar dust using Hyperion and Landsat satellite imagery for environmental monitoring in an open cast iron ore mining areas. **Journal of Cleaner Production, (Elsevier)** 218, 993-1006, SCI, Impact factor-9.29

6.1 Overview

The iron ore plays a significant role in the socio-economic development, but on the other hand, such a supply can also induce negative impact on environment and forest ecology. Dust affects the plants, physically, chemically as well as biochemically. Dust may cause a reduction in the plants growth, decrease in the production of fruit, necrosis of the leaves, and change in the community structure of the plants. So it is essential to implement forest management and environmental monitoring in surrounding mining regions. This chapter imputes the methodology for foliar dust estimation and mapping using hyperspectral satellite imagery and field obtained foliar dust data for environmental monitoring in an open cast mining areas.

6.2 Data acquisition and pre-processing

6.2.1 Data used

In this study, we had used four different remote sensing data. All of them had different sensors, bandwidths, sun angles, and different times but their spatial resolutions are the same. Two of them were multispectral data, i.e., Landsat 5/TM (2005); Landsat 8/OLI (2016), and the other two were hyperspectral data, i.e., EO-1 Hyperion (2005 and 2016). The satellite images were downloaded from the USGS website. The path and row of the satellite image scenes were 140 and 45, respectively. The secondary data were (base map, topo sheet, road network, mining plan, and forest data, and Google Earth image) collected from different sources like government offices, etc.

6.2.2 Instruments used

For foliar dust spectral signature collection, we had used a portable field Spectroradiometer. The field spectra containing 1024 bands at 1 nm (Visual), 2.5 nm (NIR), and 5 nm (SWIR) interval were then reassembled to process 198 bands using full width at half maximum (FWHM) wavelength method. For foliar dust accumulation, we had used the PCE Instrument (Model: PCE-RCM10). PCE-RCM 10 is a portable handheld particle counter used to monitor particulate dust matter (PM) concentrations in the air. This instrument has particulate matter (PM) channels: PM 2.5, PM 10, and particle sizes (in micrometers): 2.5 µm, 10 µm. Garmin Etrex20x GPS had been used to locate sample location i.e., its latitude and longitude.

6.2.3 Field survey

Dust affected forest trees and vegetation were observed and inspected during the field survey (Figure.6.1). For foliar dust estimation and vegetation change analysis, the field survey dust and spectra data were used for the justification of results.

Figure.6.1: Vegetation affected by mining generated dust in the study area

The location of foliar dust samples and unchanged areas were depicted as symbols in the study area ground survey map (Figure.6.2). During the field survey, in and around the mining area, we had noticed that the primary reason for the decline of vegetation or tree health is dust emitted by the mining activities (in this case, iron ore dust) as well as transportation of the mined out material.

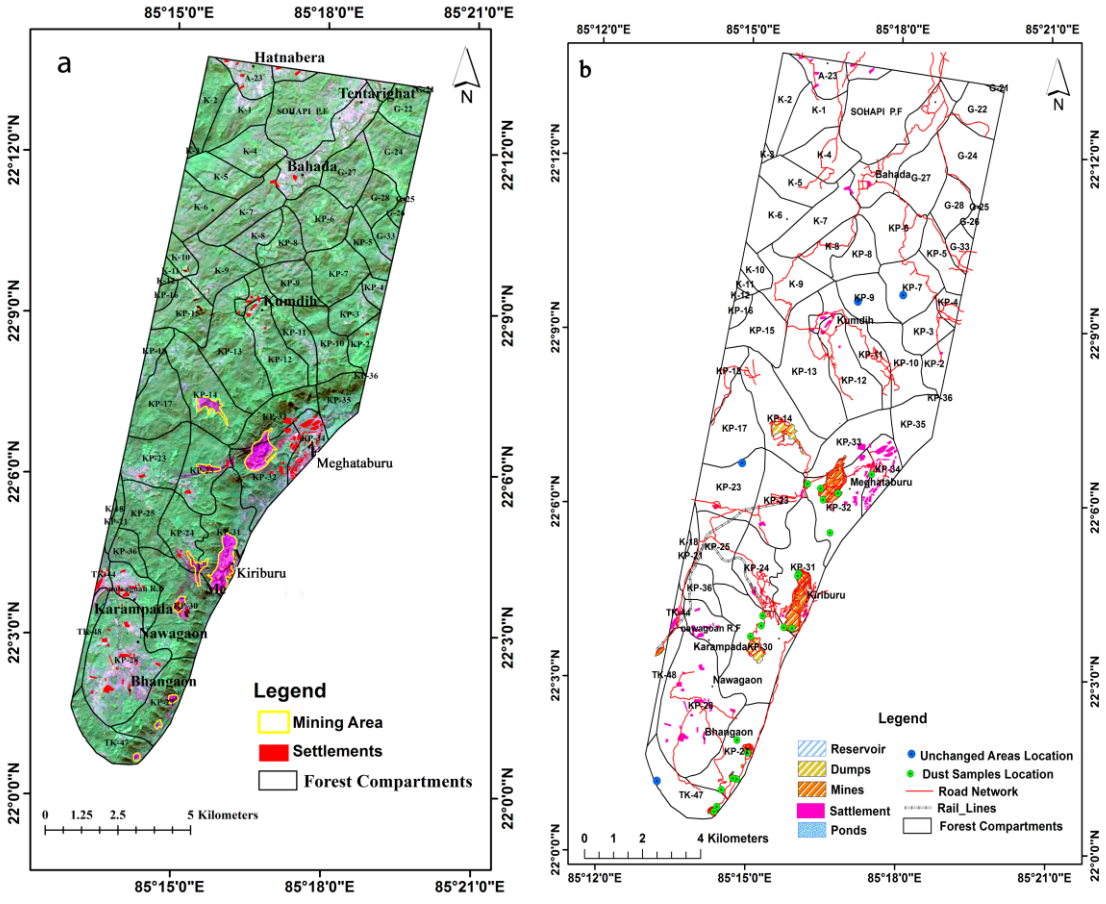

Figure 6.2: (a) Masking map used to eliminate forest and dust pixels (left) , (b) Ground truth map indicating of collected filed dust samples and unchanged areas location (Right)

At the time of field sample collection, there was no precipitation, and the weather was bright and sunny. Since remotely sensed data (via. Hyperion: narrow-bands and Landsat TM/OLI: broad-bands satellite images) were used in this study for dust appraisal, the sampling plot size was set to 30×30 meter to match the satellite images pixel size (30 ×30 meter). About 20 dust samples were collected from the study area. The location of four unchanged areas (the area not affected by dust) were recorded using GPS (Garmin Etrex20x). Field-based Spectroradiometer recorded the 20 dust affected tree leaf spectra. The field spectra were collected by a single fiber-optic light guide (SMA905) having the field of view of 180°; the purpose is to cover the compound reflectance since the dust and dust affected tree leaf are related.

6.2.4 Laboratory experiment

First, we had collected twelve to eighteen Sal and Teck tree leafs dust and cleansed the leaf with distilled water in the laboratory. Then dust was driven out by keeping it at 60 °C, and the differential weight gave the dust amount. Then the area of leaf and weight of dust were measured to analyze the weight of dust per unit area (g/m^2) a relationship was established between leaf spectra and dust amount (g/m^2). We had collected dust affected tree leaves from mining roads, tailing ponds, dumps, and mining sites. The dusty leaf spectra for each sample were recorded by field Spectroradiometer in the laboratory, and averaged spectra were used for correlation with VIs value. The dust sample was analyzed in the laboratory (Figure.6.3).

Figure 6.3: Laboratory experiment for validation

6.2.5 Landsat and Hyperion data pre-processing

Two different (Hyperspectral and multispectral) data were used for this study (Hyperion 2005 and 2016, Landsat 5/TM 2005, and Landsat 8/OLI 2016). Though both the images were from the same time, the pre-processing image method for these two (Hyperspectral and multispectral) images is the same. At first, both images were downloaded from the USGS website. Hyperion and Landsat data, both were projected to a UTM projection system at WGS 84 datum, and zone 45° north. Then they were radiometrically and

geometrically corrected. Then for atmospheric correction, the FLAASH (Fast Line-of-Slight Atmospheric Analysis of Spectral Hypercubes) module of ENVI software was used. Then band math was used to insert radiance into reflectance data. The equation for converting radiance into reflectance is given below (Equation.6.1)

$$r_\lambda = p \times L_\lambda \times d^2 / ESUN_\lambda \times \cos q_s \quad \text{(Eq-6.1)}$$

where, ρ_λ is planetary reflectance (unitless), L_λ is used spectral radiance at the sensor's aperture, d represents earth-sun distance in astronomical units, $ESUN_\lambda$ is used for mean solar atmospheric irradiances, VI_{2016} ($cosq_s$) is used for solar zenith angle in degrees.

6.3 Methodology

6.3.1 Healthy and dust contaminated areas detection

There are many causes for the degeneration of forests, such as air dust pollution, diseases, drought, soil, and weather condition. Hyperspectral remote sensing has already demonstrated its ability to detect dust and seepage contaminated forest area (Tuominen and Kuosmanen, 2008). Narrowly banded vegetation indices classes were considered for sample pixels on the field locating healthy and defoliated sample points. The healthy and defoliated pixels were used to calculate the Separability (S) choice using Equation.6.2 (Landgrebe, 2003).

$$S = \frac{u_1 - u_2}{\sigma_1 + \sigma_2} \quad \text{(Eq.-6.2)}$$

Where, mu and sigma are the mean and SD (standard deviation) of a particular healthy and unhealthy class. Separability (S) choice values have been used for vegetation combinations analysis. At first, we had analyzed VIs combination, and it was used to locate dust seepage contaminated forest and mining area. Different VIs combinations were tested, and the number of pixels classified as stressed in the healthy and contaminated dust area (%) was calculated by Equation.6.3.

$$Area_{diff} = (H - U) \quad \text{(Eq.-6.3)}$$

Where, H & U are the healthy (%) and unhealthy pixel area (%). The best VIs combination was used for classified as healthy and contaminated dust pixels.

6.3.2 Dust covered leaf spectra

Ma et al., 2017 have studied of dust covered leaves spectra with different dust amounts. In spectral reflectance study, the red wavelength region was increased because of reduced chlorophyll absorption, and the near-infrared region was decreased due to the reduced leaf cell vigor, and shifts in the red edge. We have collected leaf dust spectra with different dust amount for the foliar dust analysis.

6.3.3 Vegetation indices (VI_{diff}) for foliar dust estimating

Eight common VIs (Ma et al., 2017) were selected to estimate the foliar dust in the study area. It was used to calculate and analyze their correlation with the amount of dust covered the leaves so that according to the calibrated relationships with VI differences (VI_{diff}), the final foliar dust can be spectrally assessed. The eight common narrow banded (Hyperion) and broad-banded VIs are shown in (Table.6.1).

Table 6.1: Summary of eight narrow-banded and broad-banded vegetation indices (VIs)

VIs	Narrow bands Algorithm	Broad-bands Algorithm	Applications	References
SR (Simple Ratio)	$\frac{\rho \mathrm{NIP}_{864}}{\rho \mathrm{P}_{660}}$	$\frac{\rho NIR}{\rho R}$	It is used in this project because by knowing the vegetation status of the study area, we can analyze the change and unchanged areas between before and after mining image	C. F. Jordan, 1969
NDVI (Normalized Difference Vegetation Index)	$\frac{\rho NIR_{864}-\rho R_{660}}{\rho NIR_{864}+\rho R_{660}}$	$\frac{\rho NIR-\rho R}{\rho NIR+\rho R}$	This index is used because it has the ability to reduce many forms of multiplicative noise like sun illumination difference, cloud shadows, some atmospheric attenuation, some topographic variations that are present in multi-date imagery	Baret, & Guyot ,1991
SAVI (Soil Adjusted Vegetation Index)	$\frac{(\rho NIR_{864}-\rho R_{660})(1+L)}{(\rho NIR_{864}+\rho R_{660}+L)}$ L=0.5 in this study	$\frac{(\rho NIR-\rho R)(1+L)}{(\rho NIR+\rho R+L)}$ L=0.5 in this study	This index is widely used for minimizing the influence of soil brightness. It can be used to describe the dynamic soil-vegetation systems from satellite imagery	Huete,et al, 1988

TSAVI (Transformed Soil Adjusted Vegetation Index)	$\frac{a(\rho NIR_{864}-a\rho R_{660}-b)}{a\rho NIR_{864}+\rho R_{660}-ab+X(1+a^2)}$ a=slope of the soil line, 1.2 in this study b=soil line intercept, 0.06 in this study X=adjustment factor to minimize soil noise, 0.08 in this study	$\frac{a(\rho NIR-a\rho R-b)}{a\rho NIR+\rho R-ab+X(1+a^2)}$ a=slope of the soil line, 1.2 in this study b=soil line intercept, 0.06 in this study X=adjustment factor to minimize soil noise, 0.08 in this study	It is almost similar to SAVI to reduce the soil background effect, but it uses the parameter of the soil line. It is a modified form of SAVI to compensate for soil variability due to changes in solar elevation and canopy structure	Baret and Guyot, 1991
PVI (Perpendicular Vegetation Index)	$\frac{1}{\sqrt{1+a^2}}(\rho NIR_{864}-a\rho R_{660}-b)$ a=slope of the soil line, 1.2 in this study, b=soil line intercept, 0.06 in this study	$\frac{1}{\sqrt{1+a^2}}(\rho NIR-a\rho R-b)$ a=slope of the soil line, 1.2 in this study, b=soil line intercept, 0.06 in this study	It is used to eliminate the difference in soil background and is most effective under conditions of low LAI, applicable for arid and semiarid regions	Huete,et al, 1988
NLI(Non-Linear Index)	$\frac{(\rho^2 NIR_{864}-\rho R_{660})}{(\rho^2 NIR_{864}+\rho R_{660})}$	$\frac{(\rho^2 NIR-\rho R)}{(\rho^2 NIR+\rho R)}$	It is used for removing leaf angle distribution influence and view azimuth effect	Goel and Qin, 1994
MSR(Modified Simple Ratio)	$\frac{(\frac{\rho NIR_{864}}{\rho R_{660}})-1}{\sqrt{\frac{\rho NIR_{864}}{\rho R_{660}}+1}}$	$\frac{(\frac{\rho NIR}{\rho R})-1}{\sqrt{\frac{\rho NIR}{\rho R}+1}}$	It is a used for knowing the vegetation condition because it is less sensitive to canopy optical and geometrical properties	Chen, 1996
TC greenness(Tasselled Cap Transformation Greenness)	$-0.2787\text{Blue}_{518}-0.2174\text{Green}_{559}-0.5508\text{Red}_{660}$ $+0.7221\text{NIR}_{864}+0.0773\text{SWIR1}_{1608}-0.1648\text{SWIR2}_{2203}$	$-0.2787\text{Blue}-0.2174\text{Green}-0.5508\text{Red}$ $+0.7221\text{NIR}+0.0773\text{SWIR1}-0.1648\text{SWIR2}$	It is used to describe the amount of green biomass in the study area	Mountrakis, 2009
Note: ρR and ρNIR are reflectance in red (i.e., Landsat TM, OLI) and near-infrared (i.e., TM, OLI) wavelength respectively.				

6.3.4 VIs differencing (VI_{diff}) Landsat and Hyperion images

After pre-processing of multispectral images, eight different vegetation indices (VIs) images were extracted from the hyperspectral and multispectral data. The following eight different VIs were used to calculate and analyze their correlation with ground-based dust measurement.

As the two multispectral data (Landsat OLI and Landsat TM) were obtained under the light, and different sensor condition, there would be differences in calculating VIs. So, to overcome these problems, some unchanged areas based on field survey observation were selected to analyze the cross-image VI_{diff} by the following Equation 6.4:

$$VI_{Cross}=VI_{OLI}-VI_{TM} \quad \text{(Eq-6.4)}$$

Where, VI_{cross} is the VI diff value in the unchanged area. VI OLI and VI TM are the values calculated from Landsat OLI (2016) and Landsat TM (2005) image.

From the unchanged area samples, mean and standard deviation (σ) were calculated. The standard deviation (σ) value for different VIs of the unchanged area sample was multiplied by a constant (γ, which is from 2.5 to 3.5) which is often used to determine the threshold was used for detecting unchanged and changed vegetation in the study area (Lu et al., 2005). The constant value (γ) was set to 3.5, considering the difference in sensors, atmospheric condition, and solar illumination. For the entire image, VIcross was assumed spatially uniform. It was used to compensate the image difference because the imaging conditions between the two images were different. For calculating VI difference the following Equation. 6.5 is used.

$$VI_{Diff} = VI_{2016\,Lansat\,(OLI)} - VI_{2005\,Landsat\,(TM)} - VI_{Cross} \quad \text{(Eq-6.5)}$$

Where, VI_{Diff} is the VI difference, VI_{2005} is the VI value calculated since 2005 Landsat TM image. VI_{2016} is the VI value calculated from 2016 Landsat OLI image.

In the hyperspectral image, after pre-processing, eight different VIs images are extracted. Similarly, these eight different VIs for Hyperion image are used for calculating and analyzing their correlation with dust amount. As the hyperspectral data of the same sensor is available for determining change detection, (so no need to cross value calculation) the following Equation.6.6 is used for calculating the VI difference (VI_{Diff}).

$$VI_{Diff} = VI_{2016\,(Hyperion)} - VI_{2005\,(Hyperion)} \quad \text{(Eq-6.6)}$$

Where, VI_{Diff} is the VI difference, VI 2016 is the VI value obtained since the Hyperion satellite image of 2016 and VI 2005 is the VI value calculated from the Hyperion image of 2005.

6.3.5 VIs selection Landsat and Hyperion images

The detection of change in vegetation and its analysis in two iron mining areas is done by measuring the amount of dust accumulation on tree's leaf. The foliar dust is then estimated and on the basis of this the optimal VIs is selected.

Also, the optimal VIs will be selected based on the ground-based dust estimation result produced by comparing VI diff. based polynomial linear regression statistical model derived from the lab leaf dust spectra. The optimal VIs should have statistical criteria, such as the highest correlation coefficient (R) value and with the lowest RMSE. The following statistical equation were used for calculating the correlation coefficient (Equation.6.7), the coefficient of determination (Equation.6.8) and root mean square error (Equation.6.9).

$$R=\frac{\Sigma(x-\bar{x})(y-\bar{y})}{\sqrt{\Sigma(x-\bar{x})^2\,\Sigma(y-\bar{y})^2}} \quad \text{(Eq-6.7)}$$

$$R^2=\left(\frac{\Sigma(x-\bar{x})(y-\bar{y})}{\sqrt{\Sigma(x-\bar{x})^2\,\Sigma(y-\bar{y})^2}}\right)^2 \quad \text{(Eq-6.8)}$$

$$\text{RMSE} = \sqrt{\frac{\sum_{i=1}^{n}(P_i-O_i)^2}{n}} \quad \text{(Eq-6.9)}$$

Thus the relationship between the eight different VI and foliar dust samples were collected from the study area. VIs values were also obtained and rescaled to 0 to 1. This will help in estimating the dust differences extracted from the two Landsat images. In 2005 Landsat TM image dust amount was set to 0. Consequently 2016 Landsat OLI image, the dust volume would be given by the following Equation. 6.10.

$$D = VI_{Diff} \times L \quad \text{(Eq-6.10)}$$

Where, D is the dust volume in the year 2016 of the Landsat image, VI Diff is the VI difference between VI 2016 and VI 2005 of the Landsat image and L is a coefficient value derived from laboratory results.

In the same way as multispectral, it is essential to choose an optimal VI to estimate the better dust result in the mining area. The in situ measured value is compared with different VIs value to get the optimal VI as in the multispectral. Then the VI with the highest correlation coefficient (R) value and lowest root mean square is selected as optimal VI.

Therefore, Equation.6.10 is used to estimate the dust amount in EO-1 Hyperion image acquired in 2016. But in the case of hyperspectral data, VI difference image produced

from Equation.6.6 is used in Equation.6.10 and the coefficient value derived from the laboratory results.

6.3.6 Foliar dust estimation and accuracy assessment

The foliar dust estimation, vegetation change, and spatial patterns were analyzed for two iron ore mines sites with the help of ancillary data such as Google Earth and toposheets. The mining lease boundary, dumps, tailing ponds, local ore transportation roads were extracted from Geo-Eye satellite (Google earth image; 0.4-meter resolution) on December 5, 2016. It helps in estimating and mapping foliar dust in the mining sites. The overall accuracy of the classified class's pixels was matched to reference ground data. The classified image was calculated overall accuracy and RMSE statistic using field surveys reference dust data. By spatial pattern analysis, we compared the accuracy assessment between Landsat and Hyperion data, so that got more reliable and accurate information about foliar dust in the mining area. The overall research flow chart has been shown in Figure 6.4.

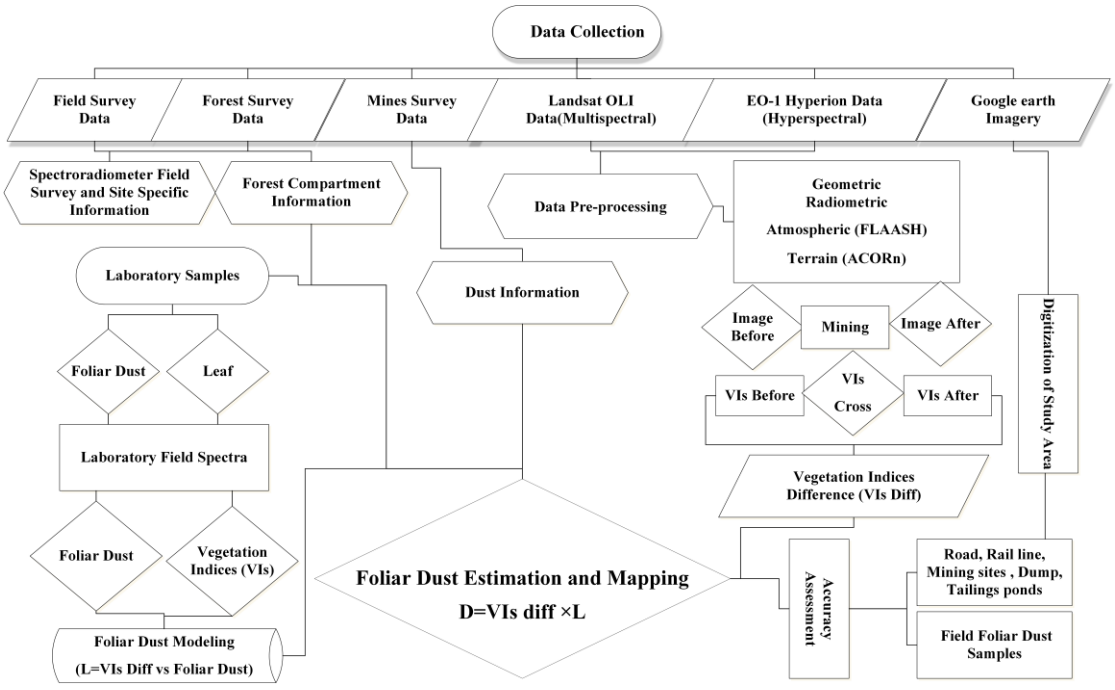

Figure.6.4: Research flowchart of foliar dust estimation and mapping

6.4 Results and Discussion

6.4.1 Field measurement of dust samples

Based on ground truth survey, the vegetation nearby the two iron ore transportation roads were significantly affected by the dust, which was emitted from the vehicles transporting mining materials. Some field photographs are given below in Figure. 6.5. About 20 dust sampling plots were collected and measured using PCE Instrument at the two iron mining sites, during the field survey. The minimum and maximum amount of dust that was measured from the sampling plots was 4.5432 g/m^2 and 55.3650 g/m^2 respectively.

Affected vegetation near the ore transportation road

Leaves covered with dust

Affected vegetation near the ore tailing pond

Figure 6.5: Vegetation affected by dust in the study area

6.4.2 Dust quality detection

20 dust samples were collected from different ground locations of two iron ore mining sites and its surrounding area. The dust samples quality were tested in geo-environmental laboratory. The dust quality samples result are shown in Table 6.2. The GPS location of the 20 sampled areas were identified and matched with the image pixel position

Table 6.2: Dust quality result of field dust samples (n=20)

Dust sample no	Latitude	Longitude	Foliar dust Account (g/m^2)	SO2 (g/m^2)	NOX (g/m^2)
1	22° 6' 12.026" N	85° 16' 47.635" E	42.86199951	70	73
2	22° 6' 5.040" N	85° 16' 29.999" E	5.350999832	BDL	46
3	22° 5' 31.050" N	85° 16' 38.574" E	7.624000072	32	52
4	22° 6' 21.250" N	85° 16' 11.081" E	6.357999802	BDL	48
5	22° 3' 52.689" N	85° 15' 44.112" E	28.45199966	67	73
6	22° 4' 4.368" N	85° 15' 18.688" E	19.315899849	56	64
7	22° 3' 42.930" N	85° 15' 4.238" E	8.475000381	35	55
8	22° 3' 54.255" N	85° 15' 17.223" E	30.63500023	63	71
9	22° 1' 55.569" N	85° 14' 49.277" E	23.57500076	57	66
10	22° 1' 42.351" N	85° 15' 2.208" E	25.36400032	61	68
11	22° 1' 15.173" N	85° 14' 49.652" E	13.5539999	45	59
12	22° 1' 4.062" N	85° 14' 31.183" E	24.53200016	59	63
13	22° 0' 46.542" N	85° 14' 25.865" E	9.425000191	38	52
14	22° 0' 41.466" N	85° 14' 22.507" E	11.23499966	41	57
15	22° 1' 15.924" N	85° 14' 44.900" E	19.56699944	54	62
16	22° 4' 48.556" N	85° 16' 1.323" E	50.81399918	78	87
17	22° 5' 19.198" N	85° 18' 4.780" E	52.35400009	82	89
18	22° 6' 16.701" N	85° 16' 26.726" E	43.25400162	71	70
19	22° 4' 45.995" N	85° 16' 0.216" E	48.52399826	74	86
20	22° 3' 51.771" N	85° 15' 54.222" E	55.36500168	85	93

6.4.3 Detection of healthy and pest inflicted defoliation pixels

The healthy and defoliated pixel's mean and standard deviation values are shown in Table.6.3. The high S (Separability) value was obtained from MNDVI705, MSI, NDNI, and CRI1. Since these VIs correlates well with the chlorophyll content, so it is obvious that its performance will be good. Due to the shadow effect of the hilly area some VIs result are showing low S (separability) values. S choice values have been used for vegetation combinations analysis.

Table 6.3: Selection of Separability (S) values for healthy and defoliated areas

Narrow band VIs	Index	Healthy Mean	Healthy Standard Deviation	Defoliated Mean	Defoliated Standard Deviation	S
Greenness Index	MNDVI705	0.66	0.03	0.17	0.08	4.21
	MSR700	0.71	0.15	0.47	0.11	1.11
	RENDVI	0.69	0.16	0.45	0.05	1.07
	REP	0.20	0.09	0.14	0.06	0.39
	VOG1	1.44	1.13	0.06	0.05	2.60
Canopy Water Content	MSI	0.53	0.05	0.32	0.146	1.03
	NDII	0.17	0.08	0.16	0.16	0.04
	NDWI	0.19	0.11	0.27	0.11	0.14
	WBI	0.77	0.05	0.26	0.10	0.93
Light Use Efficiency Index	NDNI	0.80	0.14	0.43	0.22	0.90
	PRI	0.46	0.11	0.34	0.18	0.70
	RGR Ratio	4.58	2.23	2.54	0.38	0.77
	SIPI	1.156	0.09	1.29	0.13	0.59
Leaf Pigment Index	ARI1	74.92	18.48	43.26	14.84	0.94
	CRI1	82.22	12.15	33.29	12.78	1.96
	CRI2	84.88	7.77	46.55	13.32	1.81

6.4.4 Dust and seepage detection based on VIs combinations

The results of the different vegetation indexes (VIs) combinations are shown in Table 6.4. On the basis of combinations of VIs result the forest health were classified as healthy and contaminated dust class.

Table 6.4: Percentage of pixel classified as healthy and dust contaminated areas

Narrow bands VIs Combinations	Healthy area (%)	Dust contaminated area (%)	Difference (%)
MNDVI705, MSI,NDNI,CRI1	34.29	18.56	15.73
VOG1,WBI,RGR Ratio, CRI2	27.65	12.73	14.92
MSR700,NDWI,PRI,ARI1	25.42	11.48	13.94
RENDVI,NDII,SIP1,ARI1	21.63	12.49	9.14
REP, NDII,SIP1,API1	17.21	10.72	6.49

The greenness vegetation index had the most impact on the healthy and contaminated dust pixels, and other VIs combinations were not shown the good results for healthy and contaminated dust pixels classification. Greenness VIs combination attained high value due to the high vegetation chlorophyll content. The best greenness VIs combination result was obtained with MNDVI705, MSI, NDNI, and CRI1. The healthy and contaminated dust areas classification pixels are shown in Figure. 6.6.

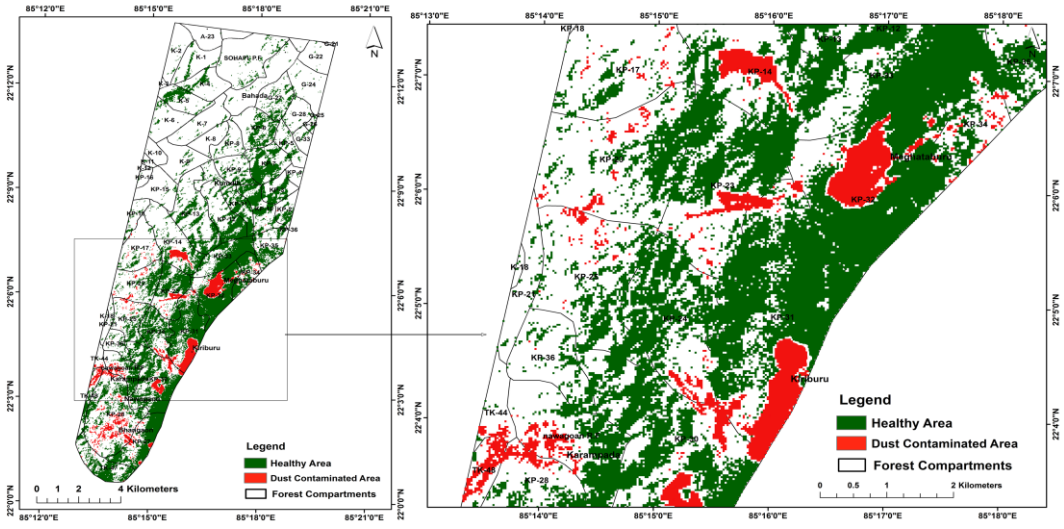

Figure 6.6: Classified healthy and dust contaminated pixels of study area

6.4.5 Relationships between foliar dust and field spectra

The relation between foliar dust and field spectra were observed and it shown the increase in amount of dust as well as red reflectance spectra and decrease in near-infrared reflectance spectra (Figure.6.7).

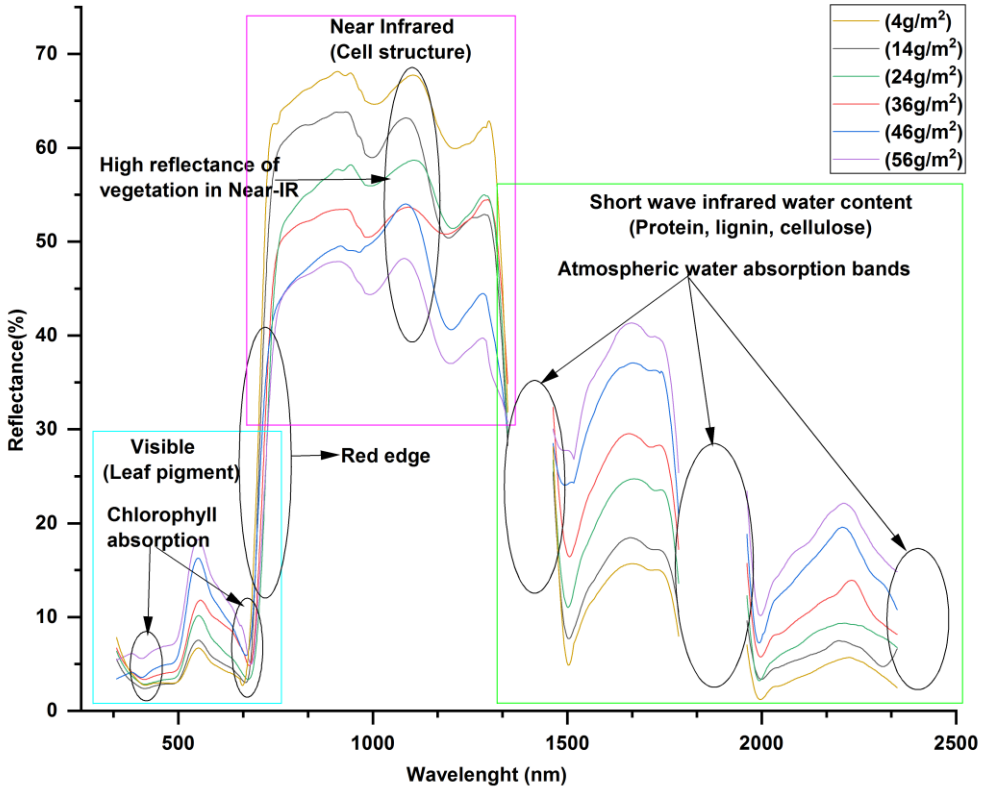

Figure 6.7: Spectral signature of dust-covered leaf with different foliar dust amounts (g/m^2)

According to the statistical results, all the VIs of both Landsat and Hyperion data were extremely correlated with dust amount. Table 6.5 shows the correlation between VIs and dust amount.

Table 6.5: Relationship between VIs value and foliar dust amounts

	Landsat		Hyperion	
VIs	Formula	R^2	Formula	R^2
MSR	y = -45.876x + 46.953	0.77	y = -46.657x + 46.592	0.83
NDVI	y = -53.124x + 52.963	0.81	y = -52.116x + 52.412	0.89
NLI	y = -42.947x + 48.025	0.64	y = -44.808x + 50.347	0.79
PVI	y = -52.468x + 45.767	0.72	y = -53.767x + 56.32	0.81
SAVI	y = -53.241x + 49.14	0.71	y = -54.944x + 55.576	0.78
SR	y = -48.974x + 48.148	0.68	y = -53.292x + 52.85	0.79
TCgreenness	y = -44.933x + 44.223	0.66	y = -48.884x + 48.14	0.74
TSAVI	y = -60.042x + 55.126	0.68	y = -60.664x + 69.56	0.75

Also, Figure.6.8 shows the statistical regression scatter plot between VIs and foliar dust amount.

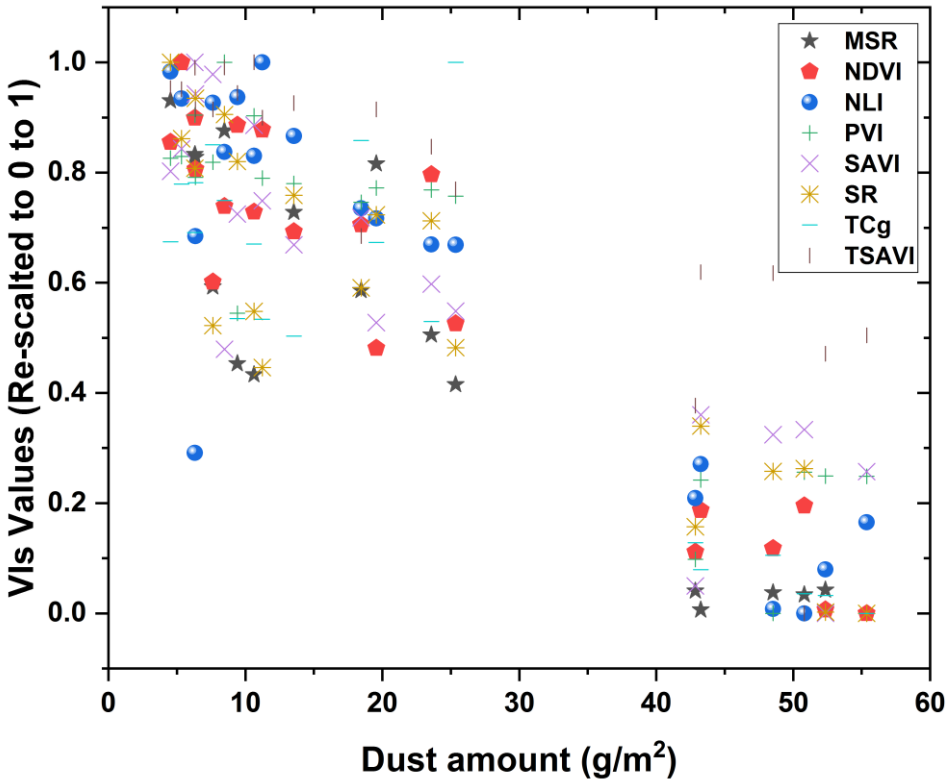

Figure .6.8: Relationship between VIs values and foliar dust amounts (g/m^2)

6.4.6 VI differences and VI selection

After performing atmospheric correction of the two images of 2005 and 2016, they were converted into surface reflectance. Then the eight common VIs of both the

images were calculated, and according to the algorithm, the VIcross image was also educed. The result of the VICross image (Hyperion and Landsat) calculated values are summarized below in Table 6.6 for unchanged area samples. The quantity of dust in the image of 2016 can be directly estimated by using the Equation.6.10.

Table 6.6: Cross-image VI difference between Landsat TM and OLI sensors for the unchanged areas

VIs	MSR	NDVI	NLI	PVI	SAVI	SR	TCgreenness	TSAVI
MEAN	0.84	0.02	0.13	0.02	0.06	0.003	0.03	0.07
SD (σ)	0.31	0.03	0.03	0.01	0.04	0.12	0.04	0.04

6.4.7 Foliar dust estimation in mining areas

In this study we have used the standard deviation (σ) value (0.0328) of the $NDVI_{diff}$ of five unchanged (2005 and 2016) area samples. A constant value was multiplied with the standard deviation (σ) value (γ, i.e., 2.5 to 3.5) and then it was used to calculate the threshold for detecting changed and unchanged vegetation (Lu et al., 2005). Furthermore, a constant value (γ) was set to 3.5, considering the two different sensors i.e., solar illumination, and atmospheric condition (Kuki et al., 2018).The dust pollution was deliberated as the primary stress issue for affecting the accrual of vegetation in the mining area. According to the laboratory result, when the dust was 55 g/m2, Landsat based NDVI was decreased to 0.2. Therefore, by using the Equation. 6.10, the Landsat based NDVI difference values from -0.3 to 0.083 (γσ) were selected for foliar dust appraisal. The Hyperion image, by using Equation. 6.10, the NDVI difference values from -0.2 to 0.076 (γσ) were selected for foliar dust appraisal. The Landsat and Hyperion based dust distribution maps were prepared by NDVIdiff image (Figure. 6.9 (a & b)).

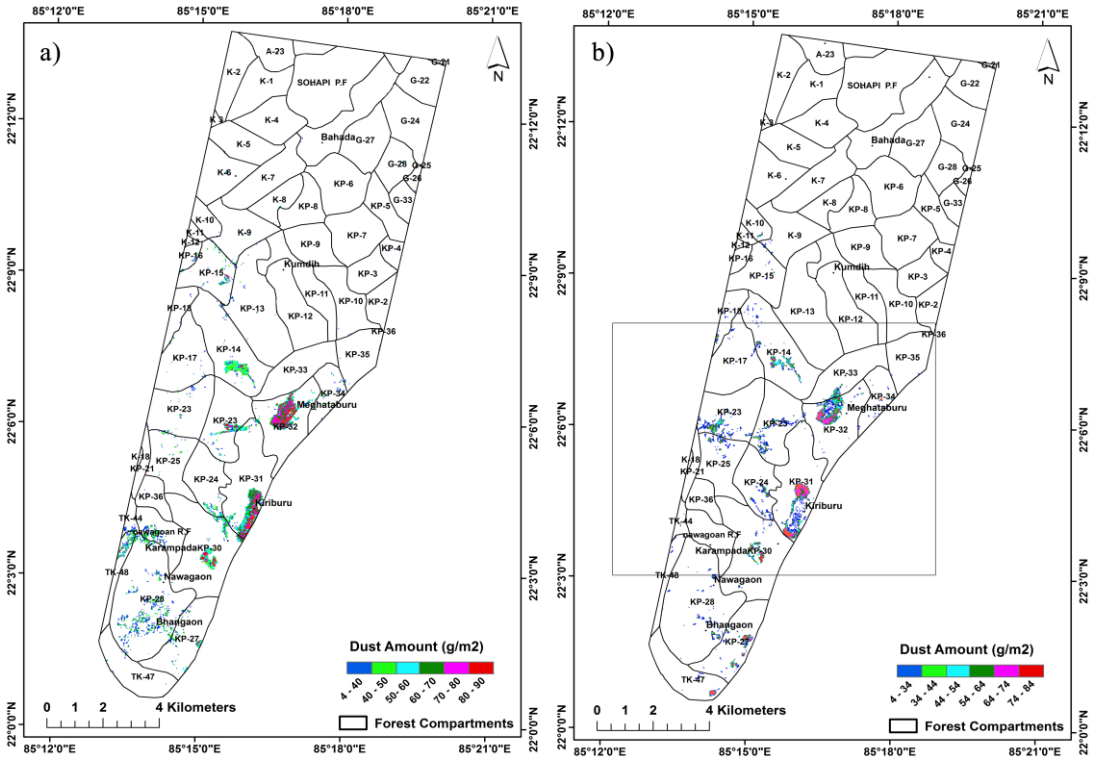

Figure 6.9: (a & b) Foliar dust mapped by Landsat (a) and Hyperion (b) data based on VIs difference dust model

The Hyperion based accuracy of the dust map was higher (RMSE = 0.06 g/m^2 and R = 0.90) than measured with Landsat data (RMSE = 0.11 g/m^2 and R = 0.81). From Google Earth, the information of roads, mining site, dumps and tailing ponds were extracted and it was found that the dusty areas were situated on both sides of the existing mining road as well as around the mining sites, tailing pond and dumps areas (Figure. 6.10).

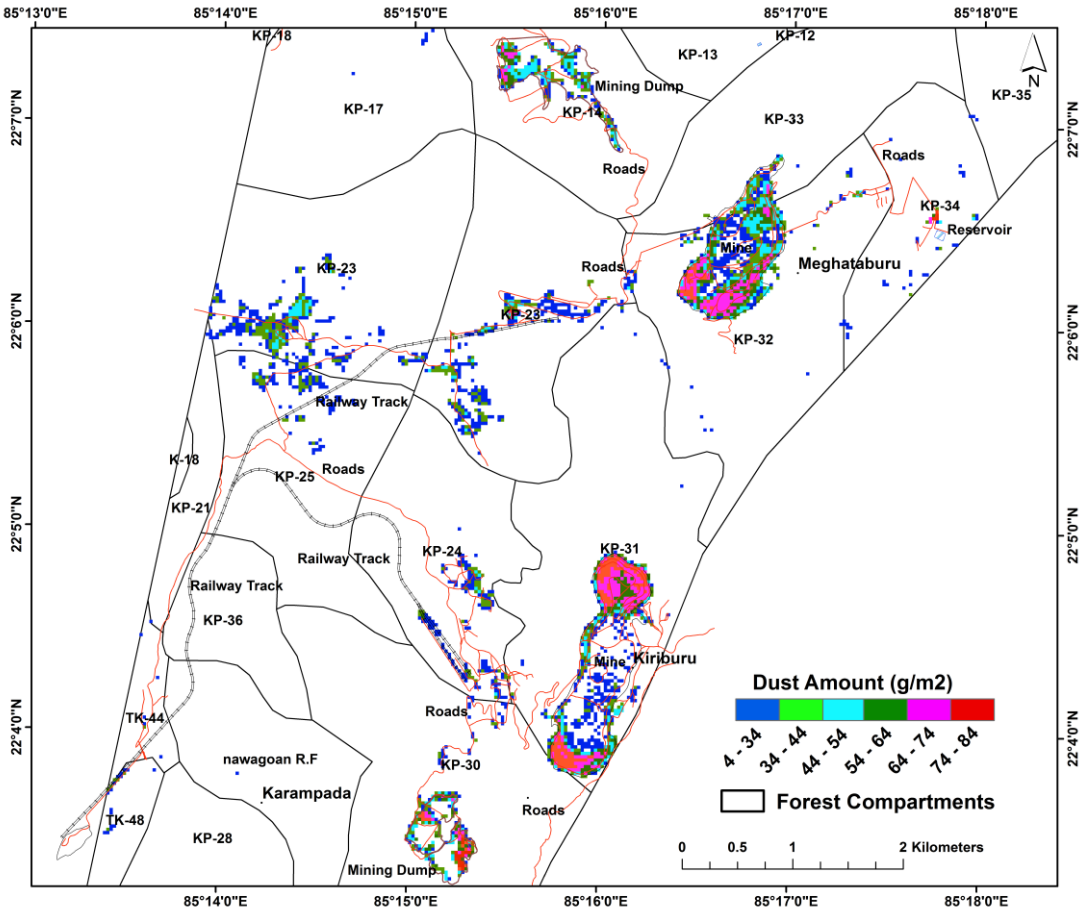

Figure 6.10: Magnified view of mines and buffer areas showing foliar dust mapped by Hyperion data

6.4.8 Relationship between distances and dust classes

The average distance of dusty area from two iron ore mines were calculated for different Hyperion based dust class (Table 6.7). A correlation study (R^2=0.79) between the average distance from mines and Hyperion based dust classification result which was calculated by the average distance for each dust classes pixels in dust contaminated areas. Results concurred with field survey studies shown that there is a clear relationship between tree's distance from mines and different dust contaminated areas.

Table 6.7: Average distance from Kiriburu and Meghataburu mines for different dust classes

Classes	Class-1	Class-2	Class-3	Class-4	Class-5	Class-6
Hyperion foliar dust amount (g/m^2)	3-34	34-44	44-54	54-64	64-74	74-80
Average distance (m)	2193	1689	1567	1340	1116	947

from Kiriburu mine						
Average distance (m) from Meghataburu mine	1439	1249	1057	910	733	639

6.4.9 Accuracy assessment

For RMS error calculation, we had used the dust value of 20 field samples. The Hyperion and Landsat images based correlation coefficient (R) and RMS error results were shown in Table 6.8 along with the scatter plot (Figure.6.11). In aforesaid table, we found that the Hyperion image estimated dust values from $NDVI_{diff}$ had the lowest RMS error (RMS error=0.06) and highest correlation coefficient (R=0.90) than the other VIs. Therefore, for dust estimation, Hyperion based NDVI was selected as an optimal VI.

Table 6.8: Accuracy of foliar dust estimation based on VIs difference (n=20)

	Landsat		Hyperion	
VI	RMSE	R	RMSE	R
MSR	0.79	0.72	0.71	0.82
NDVI	0.11	0.81	0.06	0.90
NLI	0.21	0.57	0.16	0.60
PVI	0.25	0.38	0.20	0.43
SAVI	0.31	0.51	0.23	0.59
SR	0.63	0.68	0.44	0.62
TCgreenness	0.26	0.24	0.19	0.38
TSAVI	0.28	0.56	0.21	0.69

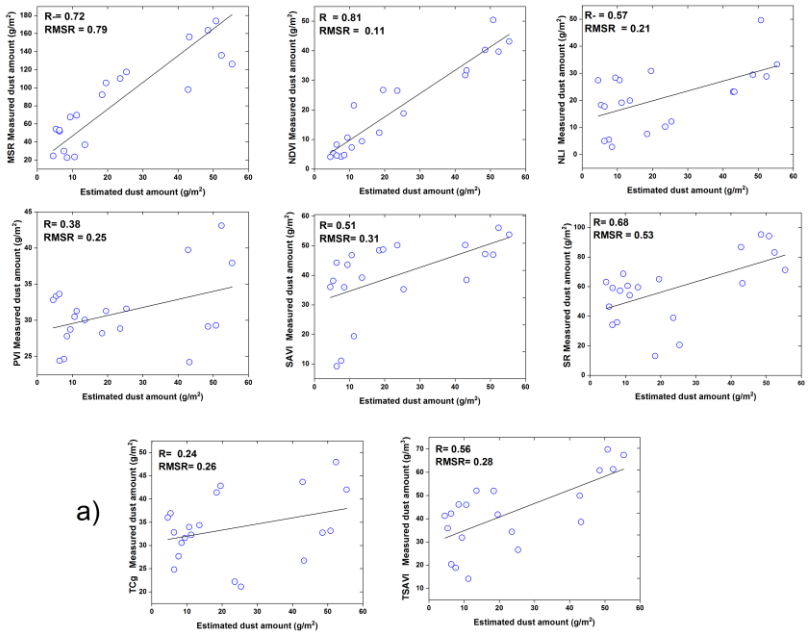

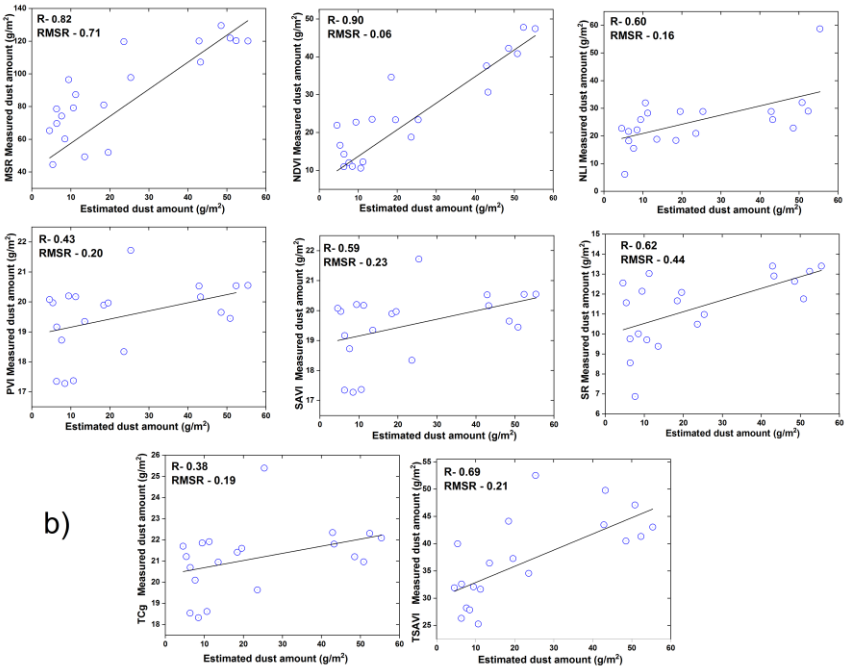

Figure 6.11: (a &b) Landsat (a) and Hyperion (b) based estimated foliar dust values of the 20 sampling plots against their measured dust values

6.4.10 Discussion

For the detection of healthy and defoliated areas, we used narrow banded VIs based separability (S) choice test. MNDVI705 correlated well with waned chlorophyll content so that this index could be used for healthy and defoliated vegetation type (Kumar et al., 2015). The MNDVI705, MSI, NDNI, and CRI1 performance are excellent because of the increased anthocyanin pigment levels. MNDVI705 and MSI offer the best separability result than the well-established NDNI and CRI1 vegetation indices. The MNDVI705 and MSI phenology growth rate is high, so it is good to perform this for the detection of defoliation (Tuominen et al., 2009; Solberg et al., 2004). By combinations of VIs result, the forest health was classified as healthy and dust affected pixels class. The vegetation indices combinations (MNDVI705, MSI, NDNI, and CRI1) had shown better results for healthy and dust affected pixels, and other VIs combinations had not shown good results for healthy and dust affected pixels (Tuominen, et al., 2008). Some earlier studies had shown the capability of getting better vegetation indices (VIs) through Hyperspectral and multispectral remote sensing (Tuominen et al., 2008 & 2009). They also propounded that separability value for NDVI (broadband) shows better results than MNDVI705 (narrowband); VIs

combination for vegetation indices for NDVI & RENDVI shows the better result for healthy and dust affected pixel.

Based on the above result, we could determine that the Hyperion based NDVI has more capability to estimate foliar dust in the mining area than any other VIs. In the study area, Sal leaves were selected as it was in abundance, for measurement of dust samples spectra in the lab that was in favor of NDVI. Therefore SAVI, TSAVI, NLI, MSR, PVI were not favoured, because various vegetation types and coverage lying from medium to high couldn't perform good tree canopy spectra (Veraverbeke et al., 2012; Jordan 1969). The statistical analysis with NDVI had given better results than other VIs. So we had used the NDVI for the study of foliar dust estimation model.

The Landsat OLI sensor is unlike the Landsat TM sensor because their bandwidths and light conditions are different. Therefore, cross-image calibration was necessary for estimating vegetation changes using VI differencing approach. The result educed from cross-image NDVI difference was 0.0328 for our study area, which was close to the result obtained by Gong et al., 2003) and Lenney et al., (1996). i.e., 0.0165 and 0.019, respectively, they had linked Landsat ETM+ with Landsat TM /OLI in their work.

However, in the case of hyperspectral data, both the images (2005 and 2016) are of the same sensor so that it might be the advantage for the Hyperion data for high accuracy than the Landsat data. Moreover, yearly climatic factors like temperature and precipitation may affect the NDVI (Wu and Wang, 2016; Wua & Yuan, 2011). The temperature of an area might be more reasonable to affect NDVI in the study area. Fortunately, the temperature and precipitation of both the year, i.e., 2005 and 2016, were almost the same and standard respectively.

Thus, in this study, the NDVI dissimilation instigated by climatic issues could be overlooked. However, in the case of NDVI difference in vegetation cover of the unchanged areas during the 11 years, the minor value (0.013) of the VIcross could be normalized and recompense the effect of the variation on the NDVI difference (Broich et al.,2011; Yan et al., 2015). Moreover, during the data collection, weather conditions must be considered because, in rainy weather, rainwater may wash away the dust on leaves. Therefore, while collecting field spectra and foliar dust data, rainy days should be avoided to confirm the validity of the data.

In the study area, the dust estimation was a significant problem because of the frequently iron ore transportation via mining haul road on a dump truck. The annual production of fine iron ore in these two mining zones are four million tons and around a thousand tons of fines per day. The mine materials get transported in nearly a thousand truck trips (Prasad et al., 2017). The day to day dust emission generated from transportation is so intensive that both sides of the road are filled with the dust, vitiating the plants and trees' health.

In this work, the RMS error of foliar dust appraisal was 0.11 g/m^2 of Landsat and 0.06 of Hyperion, which clearly shows that the dust map by Hyperion image is better than the Landsat image. The reasons behind the error in dust estimation may be because of various reasons. At first, the relationship between the dust and the NDVI difference was exhibited in a lab test. We had tested dust affected leaves spectra in the darkroom, but some noisy spectral data had come. Though, the leaf turning was more 0°, which might be contributing to dust estimation error. Secondly, in the spatial resolution of 30 × 30 meter pixel area, there might exist road surfaces with dust along the sides which were covered with the dense forest of Sal or teak tree or different vegetation. Those pixels are known as mixed pixel because it includes different components within one pixel (Lee et al., 1980). Thus, the estimation of the dust amount from the pure pixel will be different from the mixed pixel.

6.5 Summary

Due to several factors, the plants of the study area are affected by iron ore dust. So for monitoring the dust on plants or in the forest, we measured the foliar dust with the help of satellite imagery and field based dust measurement. We also compared the outcome of Hyperspectral and Multispectral data to find the reliability of the NDVI based dust model. Moreover, this methodology could be employed in other mining-affected regions, considering the dust sample variance.